SUPPLEMENTARY FIGURE LEGENDS

Figure S1. Activation-dependent binding of kinases to Multiplexed Inhibitor Beads (MIBs). Related to Figure 1

(A) Structures of kinase inhibitors conjugated to beads used as Multiplex Inhibitor Beads.

(B) Increased binding of EGFR signaling components following EGF stimulation. SILAC labeled MDA-MB-231 cells were serum starved overnight and stimulated with 30 ng/ml EGF for 15 min, harvested and applied to MIBs. A SILAC-based quantitative comparison of MIB-bound kinases from serum starved versus EGF stimulated cells was performed.

(C) Increased binding of tyrosine kinases to MIBs following pervanadate phosphatase inhibitor treatment. SILAC labeled chronic myeloid leukemia cells (MYL) were treated with 100 μM pervanadate for 15 min, harvested and kinome isolated using MIBs. A SILAC-based comparison of MIB-bound kinases in the presence or absence of pervanadate was determined.

Figure S2. **Kinome profile of MDA-MB-231 TNBC cells in response to MEK1/2 inhibition. Related to Figure 2**

(A) MDA-MB-231 cells are growth inhibited by 5 μM U0126 or AZD6244. Triplicate experiments $\pm$ SD.

(B) Inhibition of ERK1/2 activity in MDA-MB-231 cells in response to 5 μM U0126 or AZD6244 treatment for 4 or 24h.

(C) Kinase phosphorylation is altered in response to AZD6244 treatment. SILAC-labeled SUM159 cells were treated with 5 μM AZD6244 and changes in pSer, pThr, and pTyr phosphopeptides were identified by TiO_2 enrichment of MIB elutions.

(D) Induction of PDGFRβ in response to MEK1/2 inhibition in MDA-MB-231 cells. SILAC labeled cells were treated with 5 μM U0126 or AZD6244 for 24h, harvested and kinases isolated using MIBs. Quantitative comparison of MIB-bound kinases treated with MEK1/2 inhibitors compared to DMSO treated cells.

(E) Increased RTK activity in claudin-low cell lines following inhibition of MEK1/2. SUM159 and MDA-MB-231 cells were treated with 5 μM U0126, AZD6244 or DMSO for 24h and analyzed using RTK arrays.

(F) Top 40 kinases expressed in patient claudin-low tumor. RPKM values for each kinase determined by RNA-seq. *denotes AZD6244-responsive kinase in SUM159/MDA-MB-231 cell profiling.

(G) Pairwise plot of the log2 protein ratio (negative log p-values) for the replicates and the pooled data. The Pearson correlation coefficients printed in the upper corner indicate high reproducibility of the MIB kinase affinity capture technique.

(H) Pairwise plot of the negative log p-values for the replicates and the pooled data. The Pearson correlation coefficients printed in the upper corner indicate high reproducibility of the MIB kinase affinity capture technique.

(I) Overlap/concordance between the individual MIB/MS replicates. Concordance was greater than 70% among the top 20 kinases and was higher between pooled data and each of the individual replicates.

(J) Venn diagram of the overlaps between the lists of significant kinases from MIB/MS replicates.

Figure S3. Transcriptional upregulation of RTKs and cytokines in MDA-MB-231 cells and specificity of kinome response. Related to Figure 3

(A) MDA-MB-231 cell response to AZD6244 parallels SUM159 response.

(B) Transcriptional upregulation of kinases following 5 μM AZD6244 treatment in MDA-MB-231 cells, as determined by qRT-PCR.

(C) Transcriptional upregulation of cytokines following 5 μM AZD6244 treatment in MDA-MB-231 cells, as determined by qRT-PCR.

(D) Return of cyclin expression in SUM159-R cells compared to SUM159 cells treated with AZD6244, as determined by qRT-PCR.

(E) SUM159 cells are growth inhibited by U0126 (5 μM), AZD6244 (5 μM), and BEZ235 (50 nM).

(F) BEZ235 inhibits p70 S6 kinase activity but not ERK1/2 signaling in SUM159 cells.

(G) Treatment of SUM159 cells with BEZ235 (50 nM) induces a distinct kinome response compared to AZD6244 or U0126 (5 μM), as determined by MIBs/MS using iTRAQ. Drug treatments are standardized to untreated SUM159 cells, and only kinases with statistically significant changes (pvalue<0.1) are shown.

Error bars represent triplicate experiments ± SD.

Figure S4. c-Myc loss causes induction of RTKs. Related to Figure 4

(A) Stable suppression of c-Myc protein levels following AZD6244 treatment. SUM159 and MDA-MB-231 cells were treated with 5 μM AZD6244 over 48h and c-Myc protein determined by western blot.

(B) IP of c-Myc from cells and subsequent blotting with the p-c-Myc S62 antibody shows loss of c-Myc phosphorylation in cells treated with AZD6244.

(C) Antibodies targeting either the N- or C-terminus of c-Myc identify single bands for c-Myc and phospho-c-Myc S62 that are inhibited by 72h treatment with 5 μM AZD6244.

(D) ChIP-PCR with c-Myc antibody shows enrichment for c-Myc at PDGFRβ promoter in SUM159 cells.

(E) RNAi knockdown of c-Myc for 72h in SUM159 cells induces an RTK tyrosine phosphorylation similar to AZD6244 treatment with an increase in PDGFRβ and VEGFR2 phosphorylation.

(F) siRNA-mediated knockdown of both ERK1 and ERK2 suppresses c-Myc expression and causes induction of PDGFRβ transcript, as determined by qRT-PCR.

(G) PI3K/mTOR inhibition by BEZ235 (100 nM) does not affect c-Myc protein levels, as determined by western blot.

(H) Treatment of SUM159 cells with 3 μM GSK3 inhibitor X (GSK3X) for 24h stabilizes c-Myc in the presence of 5 μM AZD6244, suppressing PDGFRβ induction.

(I) Stabilization of c-Myc by bortezomib prevents AZD6244-dependent induction of RTK transcript, as shown by qRT-PCR. SUM159 cells were treated with AZD6244 (5 μM) or bortezomib (10 nM) alone or in combination for 24h.

(J) qRT-PCR of SUM159 cells treated with AZD6244 (5 μM) and/or bortezomib (10 nM). Inhibition of the proteasome with bortezomib prevents AZD6244-mediated loss of c-Myc transcript.

(K) Treatment of SUM159-R cells with bortezomib (10 nM) stabilizes c-Myc transcript to near-wildtype levels.

(L and M) Bortezomib treatment of SUM159-R cells stabilizes c-Myc and reverses RTK reprogramming. SUM159-R cells were treated with 10 nM bortezomib for 24h and c-Myc protein levels and reversal of RTK induction shown by (L) western blot and (M) qRT-PCR.

(N) Removal of AZD6244 results in stabilization of c-Myc protein and reversal of RTK reprogramming. AZD6244 was removed from the media of SUM159-R cells over a 72h period and RTK reprogramming determined by western blot.

(O) Washout of AZD6244 from SUM159-R causes reduction in RTK and cytokine transcript, shown by qRT-PCR.

(P) Washout of AZD6244 restores c-Myc RNA levels. AZD6244 was removed from the media of SUM159-R cells and c-Myc RNA levels determined by qRT-PCR over 72h.

(Q) Recovery of c-Myc stability and Myc:Max heterodimers in SUM159-R cells. Max IP from SUM159 cells shows Myc:Max heterodimerization is inhibited at 4h and 72h of 5 μM AZD6244 treatment, but not in SUM159-R cells. The recovery of c-Myc transcript and Myc:Max heterodimerization in SUM159-R correlates to the partial suppression of RTKs in SUM159-R cells compared to SUM159 cells acutely treated with AZD6244.

Error bars represent triplicate experiments ± SD.

Figure S5. Combination of AZD6244 with tyrosine kinase inhibitors in SUM159 and MDA-MB-231 cells. Related to Figure 5

(A) Synthetic lethal-like responses in MDA-MB-231 upon knockdown of induced RTKs in the presence of U0126. LYN and EPHA2 are negative controls not induced by U0126.

(B) Growth inhibition and synthetic lethal-like responses of siRNA-mediated knockdown of MAPK components or PI3K/AKT in SUM159 cells in the presence of U0126.

(C) Target knockdown with deconvolved siRNA pools of PDGFRβ and (D) DDR1 in SUM159 cells shows enhanced lethality with knockdown in the presence of AZD6244. Cells were treated with 5 μM AZD6244 and siRNA for 96h and subjected to cell counting. Knockdown was determined by qRT-PCR.

(E) AZD6244 synergizes with sorafenib to inhibit MDA-MB-231 cell growth.

(F) Combination of AZD6244 and foretinib has little effect on MDA-MB-231 cell growth.

(G) Cotreatment of MDA-MB-231 cells with AZD6244 and sorafenib for 72h inhibits AZD6244-mediated tyrosine phosphorylation of PDGFRβ.

(H) Western blotting shows enhanced BIM expression and cyclin D1 loss with combined AZD6244/sorafenib treatment (72h) in MDA-MB-231 cells.

(I) Cotreatment of SUM159 cells with AZD6244 and sorafenib for 72h synergizes to inhibit cell growth better than the combined treatment with AZD6244 and targeted RAF inhibitors PLX4720 or SB590885.

(J) Cotreatment of SUM159 cells with AZD6244 and sorafenib for 72h synergizes to inhibit cell growth better than the combined treatment with AZD6244 and targeted RAF inhibitors PLX4720 or SB590885.

Error bars represent triplicate experiments ± SD.

Figure S6. AZD6244 kinome response signature in C3Tag GEMM. Related to Figure 6

Induction of PDGFRβ expression in tumors from two independent C3Tag mice following 2d treatment with 20 mg/kg AZD6244 shown by immunofluorescence (DAPI is grayscale). Representative fields of tumors shown.

Figure S7. Combined treatment of AZD6244 and sorafenib synergize to promote apoptosis in C3Tag GEMM. Related to Figure 7

(A) Tumor volumes of C3Tag breast tumors during a 21d time course of AZD6244 and/or sorafenib treatment.

(B) Increased apoptosis in tumors from three distinct C3Tag mice following 2d treatment with AZD6244 and/or sorafenib compared to untreated mice, as shown by TUNEL staining in red (DAPI is grayscale). Representative fields of tumors shown.

SUPPLEMENTARY PROCEDURES

Cell culture

MYL CML cells were cultured in RPMI 1640 medium (Invitrogen, Carlsbad, CA) supplemented with 10% fetal bovine serum (Atlanta Biologicals, Norcross, GA) and 1% antibiotic/antimycotic (Invitrogen). For SILAC labeling, MYL cells were grown for five doublings in arginine- and lysine-depleted media (as above) supplemented with either unlabeled L-arginine (84 mg/L) and L-lysine (48 mg/L) or equimolar amounts of [$^{13}C_6$,$^{15}N_4$]arginine (Arg^{10}) and [$^{13}C_6$]lysine (Lys^6) (Cambridge Isotope Laboratories) as described previously (Ong SE, 2002).

Generation of immortalized T2-C3Tag cell line from a C3Tag tumor

An autochthonous tumor from a C3Tag mouse was excised and dissociated in a sterile fashion in the presence of 0.25% trypsin (Gibco). Cells were then passed through a 40 micron cell strainer and grown in the presence of DMEM + 10% FBS. Cells were isolated and expression of SV40T antigen verified by immunoblotting with antibodies specific to SV40 large T (EMD Biosciences, monoclonal, clone PAb416).

Compounds

Sorafenib and U0126 were purchased from LC Labs. BEZ235 was purchased from Selleck, Bisindoylmaleimide-X was from Alexis and Purvalanol B was from Tocris. GSK3 Inhibitor X was obtained from Calbiochem. Foretinib and AZD6244 were synthesized according to the procedures described in two patent applications (WO2005030140A2, WO2007002157A2). PP58 (Klutchko, 1998), VI16832 (Daub et al., 2008) Dasatinib (Das J., 2006), Lapatinib (Barker, 2001), SB203580 (Gallagher, 1997), PLX4720 and SB590885 were custom synthesized according to previously described methods by The Center for Combinatorial Chemistry and Drug Discovery, Jilin University, P.R. China.

RNA sequencing

Polyadenylated (poly-A) mRNA was isolated from 10 μg total RNA using Dynal oligo(dT) beads (Invitrogen). Poly-A mRNA was fragmented for five minutes at 70°C using Fragmentation buffer from Ambion. First strand cDNA synthesis used random hexamer primers and SuperScriptII (Invitrogen). Second strand cDNA synthesis was performed using DNApolI (Invitrogen) and was purified using QIAquick PCR spin columns (Qiagen). Library preparation was performed according to manufacturer's instructions (Illumina).

RNA-seq alignment and transcript expression analysis

76-bp Illumina RNA-seq reads for a claudin-low tumor (3 lanes), SUM159 (4 lanes), and MDA-MB-231 (3 lanes) were obtained from the TCGA and aligned to the UCSC human knownGene mRNA from NCBI build 37 (hg19) using Bowtie (Langmead, 2009). The alignment was performed allowing just one mismatch in each read and only the best resulting alignment was reported for each aligned read. Duplicate reads were removed using Picard (http://picard.sourceforge.net) and in-house scripts were used to obtain read counts for protein kinases. Read counts were summed for all isoforms of each kinase gene. The raw kinase transcript read counts were then normalized with a calculation of reads per kilobase of exon model per million mapped reads (RPKM) (Mortazavi, 2008). The value of "N" (total number of mappable reads) in the RPKM formula was defined as the total number of aligned reads minus the duplicate reads. Additionally, the mean isoform length for each gene was used in the RPKM calculations. All read counts and RPKM values for each cell type are in TableS1.

Western blotting

Proteins from cell lysates were separated by SDS-PAGE chromatography, transferred to nitrocellulose membranes, and probed with the indicated primary antibodies. Antibodies recognizing pAKT (S473), pAKT (T308), pAXL (Y702), AXL, c-Myc, DDR1, EGFR, pERK1/2 (T202/Y204), pHER3 (Y1197), MAX, pMEK1/2 (S217/S221), MEK1/2, MKP3, pP70S6K (T389), pPDGFRβ (Y751), pPDGFRβ (Y1009), pPDGFRβ (Y857), PDGFRβ, pRAF (S338), pRSK1

(T359/S363), pVEGFR2 (Y1175), VEGFR2 were obtained from Cell Signaling Technology. Antibodies for c-Myc (C-terminal), Cyclin A2, Cyclin B1, Cyclin D1, ERK2, MEK2 and RAF were obtained from Santa Cruz Biotechnology. The antibody recognizing Bim was obtained from Chemicon. The antibody recognizing p-c-Myc (S62) was obtained from Abcam. Secondary HRP-anti-rabbit, HRP-anti-mouse and HRP-anti-goat secondary antibodies were from Jackson Immunoresearch Laboratories, GE Healthcare and Santa Cruz Biotechnology, respectively. Western blots were visualized by incubation with SuperSignal West Pico Chemiluminescent Substrate (Thermo Scientific).

RTK arrays

Cells were harvested in RTK array lysis buffer containing 20 mM Tris-HCl (pH 8.0), 1% NP-40, 10% glycerol, 137 mM NaCl, 2 mM EDTA, 1X EDTA-free protease inhibitor cocktail (Roche), and 1% each of phosphatase inhibitor cocktails 1 and 2 (Sigma). After incubating on ice for 20 minutes, cell debris was pelleted at 4°C. Lysates (500 μg protein) were applied to R&D Systems Proteome Profiler™ Human Phospho-RTK antibody arrays. Washing and secondary antibody steps were performed according to the manufacturer's instructions. RTK arrays were visualized by SuperSignal West Pico Chemiluminescent Substrate (Thermo Scientific).

Generation of c-Myc(T58A) SUM159 and T2-C3Tag Cells

Phoenix cells were transfected with either pMSCV Myc(T58A) puro (Addgene Plasmid 18773) or empty vector pMSCV. Retrovirus-containing media was filtered 48h post-infection after addition of polybrene (6 μg/ml), and placed on SUM159 and T2 cells for 36h. After an additional 4d in fresh media, cells were selected in either 3 μg/ml (SUM159) or 6 μg/ml puromycin (T2-C3Tag) for one week. Selected cell populations were used in subsequent experiments.

ChIP-PCR

Cells were fixed for 10 min in 1% formaldehyde, sonicated (VCX130 Ultrasonicator), and immunoprecipitated with 5 μg anti-c-Myc and protein A dynabeads (Invitrogen). Crosslinking was reversed by overnight incubation at 65°C, and DNA was purified with the MinElute PCR purification kit (QIAGEN). ChIP assay was quantified by real-time PCR using Absolute Blue SYBR green PCR mix (Thermoscientific). Fold enrichment was determined by the $2^{-\Delta CT}$ method using the following PCR primers designed to amplify 75-100 bp fragments from genomic DNA: forward 5'-GGCTTTGAGACGTGAAAAGGA-3' and reverse 5'-

GGTCATCCAGCACAGATTGGA-3’; forward 5’-TGGGCCTTGGTTTGTCCTT-3’ and reverse 5’-CATGGAGGAGATGGAAAGATCCT-3’.

Inhibitor-conjugated bead preparation

Inhibitor beads were prepared via carbodiimide coupling of kinase inhibitors to ECH Sepharose 4B (Lapatinib, Bisindoylmaleimide-X, SB203580, Dasatinib, PP58 and VI16832) or EAH Sepharose 4B (Purvalanol B) (GE Healthcare). Briefly, ECH-Sepharose and EAH-Sepharose beads were washed with 50% DMF/EtOH followed by incubation with kinase inhibitors in 50% DMF/EtOH and 0.1M EDC (Sigma) at pH 5-6 overnight at 4°C in the dark. Following coupling, excess remaining groups were blocked with 0.1M N-ethyl-N’-(3-dimethylaminopropyl) carbodiimide hydrochloride (EDC) in 50% DMF/EtOH 1M ethanolamine (ECH-Sepharose) or 20 mM HAc in 50% DMF/EtOH (EAH-Sepharose). Subsequently, beads were washed with 50% DMF/EtOH and alternating washes of 0.1 M Tris-HCl (pH 8.3) and 0.1 M acetate (pH 4.0) buffers, each containing 0.5 M NaCl. Inhibitor beads were stored in 20% ethanol at 4°C in the dark.

Multiplexed inhibitor bead affinity chromatography

Cells were lysed on ice for 20 minutes in lysis buffer containing 50 mM HEPES (pH 7.5), 0.5% Triton X-100, 150 mM NaCl, 1 mM EDTA, 1 mM EGTA, 10 mM sodium fluoride, 2.5 mM sodium orthovanadate, 1X protease inhibitor cocktail (Roche), and 1% each of phosphatase inhibitor cocktails 2 and 3 (Sigma). Cell lysate was sonicated (3x10s) on ice and centrifuged for 15 min (13,000 rpm) at 4°C and the supernatant was collected and syringe-filtered through a 0.2 μM SFCA membrane. The filtered lysate (approximately 20-40 mg of protein per experiment) was brought to 1M NaCl and pre-cleared by flowing over 500 μl of blocked and washed NHS-activated Sepharose 4 Fast Flow beads (GE Healthcare). The flow-through was collected and passed through a column of layered inhibitor-conjugated beads (Bisindoylmaleimide-X (50 μl), SB203580 (50 μl), Lapatinib (100 μl), Dasatinib (100 μl), Purvalanol B (100 μl), VI16832 (100 μl), PP58 (100 μl)) to isolate protein kinases from the lysates. Kinase-bound inhibitor beads were washed with 20 ml of high-salt buffer and 10 ml of low-salt buffer, each containing 50 mM HEPES (pH 7.5), 0.5% Triton X-100, 1 mM EDTA, 1 mM EGTA, and 10 mM sodium fluoride, and 1M NaCl or 150 mM NaCl, respectively. A final wash of 1 ml 0.1% SDS was applied to the columns before elution in 1 ml of a 0.5% SDS solution in high heat. Elutions from all columns were combined and cysteines were alkylated by sequential incubations with DTT (final concentration 5 mM) for 20 min at 60° C and iodoacetamide (final concentration 20 mM) for 30 min at room temperature in the dark. The elution was spin-concentrated to 100 μl and detergents were removed by a chloroform/methanol extraction. Briefly, 400 μl of HPLC-grade methanol, 100 μl HPLC-grade chloroform, and 300 μl HPLC-grade water was added to the 100 μl concentrated elution, with vortexing and centrifugation at 13,000 rpm between each addition. After a final mixing, the sample was centrifuged for 5 min to pellet the protein at the interface and the upper phase was removed with care to leave the protein pellet intact. The protein pellet and lower phase were resuspended in 300 μl of methanol, and the sample was again vortexed and centrifuged for 5 min to pellet the protein at the bottom of the tube. The supernatant was removed and one or more methanol washes were performed to ensure the removal of detergents.

MIB statistical analysis

Data obtained from the MALDI TOF/TOF was processed with the ProteinPilot software to identify proteins from database searches and quantify changes in binding of kinases to MIBs using the Paragon Algorithm. The search results are further processed by the Pro Group Algorithm to determine the smallest justifiable set of detectable proteins and relative protein levels. We performed three replicates of SILAC labeled SUM159 cells treated with AZD6244 (2 'heavy', 1 'light') or DMSO to assess the reproducibility of MIB kinase affinity capture. A total of 113 unique kinases are identified. For each kinase, we computed the pool protein ratio and p-value across the three replicates as follows. Let y_{ij} denote the log2 protein ratio for kinase i, i=1, …,113 in replicate j, j=1,2,3. The pool protein ratio for kinase i is defined as $2^{\wedge}y_i$, where $y_i=(\Sigma^3_{j=1}y_{ij})/3$. To avoid directional conflict, we convert the two-sided p-value reported in ProteinPilot to one-sided p-value and denote it as p_{ij}. We apply Stouffer's z-score method to combine the p-values. Let $z_{ij}=\Phi^{-1}(1-p_{ij})$, where Φ is the standard Gaussian cumulative distribution function. Define the combined Z-score as $z_i=(\Sigma^3_{j=1}z_{ij})/\sqrt{3}$. The combined two-sided p-value for kinase i is given as $p_i = 2(1-\Phi(|z_i|))$. We also assessed the overlap/concordance between the kinases ranked by p-values for any two pairs of replicates. For each replicate, we identified kinases which exhibit statistically significant changes in expression based on Benjamini-Hochberg adjusted p-values at FDR of 0.05 to account for multiple comparisons. 24, 13 and 10 kinases are identified to be statistically significant for replicate 1, 2 and 3, respectively. 24 kinases are identified to be statistically significant in the pooled p-values, and are listed in Table S6. Statistical analysis for determining MIB-binding signatures is illustrated in Figures S2G-J.

Cell viability assays using siRNA knockdown of protein kinases

siGENOME pooled siRNAs for the genes of interest were obtained from Dharmacon, Thermo Scientific. RNAi assays were performed in either 96- or 384-well clear bottom plates. Prior to the assay, transfection conditions were optimized for SUM159 or MDA-MB-231 cells using Dharmafect transfection reagent and siRNAs for GAPDH (negative control), and UBB (lethality control). A 40 μl mixture of Dharmafect and siRNA was plated into each well by a multi-channel pipette and then followed by adding 160 μl cell suspension using a microplate dispenser. The final assay volume was 200 μl with a dose of 25 nM siRNA. Drug or vehicle solvent was added to the cell suspension before plating the cells. The assay was performed in triplicate and each plate had quadruple positive (UBB) and negative (GAPDH) controls. After 96h incubation at 37°C with 5% CO_2, the number of viable cells in each well was determined by a luminescence viability assay with a Pherastar microplate reader. The % activity was calculated against the averages of positive and negative controls (% activity = 100 x (1 - [raw value - σ_p]/[σ_n - σ_p], where σ_p and σ_n are averages of raw values for the positive and negative controls, respectively. Each median in triplicate was used as a representative of % activity in the figures. Two-to-three independent experiments were performed with each cell line and siRNA.

Phosphoproteomics analysis of MIBs

Phosphopeptides were enriched from MIB elution digests using TiO_2 beads as previously described (Thingholm, 2006). Tryptic peptides were separated by reverse phase nano-HPLC using a nanoAquity UPLC system (Waters Inc). Peptides were first trapped in a 2 cm trapping column (75 μm ID, C18 beads of 2.5μm particle size, 200 Å pore size) and then separated on a self-packed 25 cm column (75 μm ID, C18 beads of 2.5μm particle size, 100 Å pore size) at room temperature. The identity and phosphorylation status of the eluted peptides was determined with a Velos-Orbitrap mass spectrometer (Thermo-Scientific). Specifically, following a FT full scan, MS^2 spectral data were acquired by one of three dissociative methods on the 9 most intense ions from the full scan, taking into account dynamic exclusions. For ion dissociation, collision induced dissociation (CID), high energy collision induced dissociation (HCD) or a CID/HCD toggle was employed. The polysiloxane lock mass of 445.120030 was used throughout.

All raw data were converted to mzXML format and then searched using Sequest on a Sorcerer 2.0 platform (Sage N Research, Milpitas, CA). The search was semi-tryptic on the human IPI database (10/3/2010) appended with reversed sequences as decoys. Dynamic modifications for phosphorylated serines, threonines, and tyrosines were used, as well as a static modification for carbamidomethylated cysteines. Another search was also performed with the SpectraST algorithm provided in the Transproteomic Pipeline (TPP) version 4.4.1 using the NIST human ion trap database (1/14/2010). Results from the Sequest and SpectraST searches were analyzed using TPP's PeptideProphet and then combined using IProphet (Shteynberg, et al. 2008). SILAC ratios were calculated with the XPRESS algorithm within TPP. XPRESS parameters were heavy arginines' with a mass difference of 10 and heavy lysines' with a mass difference of 6. Protein identifications were output by TPP's ProteinProphet.

Immunofluorescence and TUNEL assays

Tumors were snap frozen, cryosectioned at 6 μm and fixed in 4% paraformaldehyde for 15 min. Sections mounted on glass slides were incubated overnight with PDGFRβ rabbit antibody (Cell Signaling #3169) at 1:1000 dilution. Secondary antibody was Alexa 555 goat-anti rabbit. Protocol provided by Cell Signaling for staining of cryosections was followed. TUNEL assays were performed using the In Situ Death Detection Kit per manufacturers protocol (Roche, #12156792).

References

Barker, A.J., Gibson, K. H., Grundy, W., Godfrey, A. A., Barlow, J. J., Healy, M. P., Woodburn, J. R., Ashton, S. E., Curry, B. J., Scarlett, L., Henthorn, L., and Richards L. (2001). Studies Leading to the Identification of ZD1839 (IressaTM): An Orally Active, Selective Epidermal Growth Factor Receptor
Tyrosine Kinase Inhibitor Targeted to the Treatment of Cancer. Bioorganic & Medicinal Chemistry Letters *11*, 1911-1914.

Das J., C., P., Norris, D., Padmanabha, R., Lin, J., Moquin, R. V., Shen, Z., Cook, L., S., Doweyko, A. M., Pitt, S., Pang, S., Shen, D. R., Fang, Q., de Fex, H. F., McIntyre, K. W., Shuster, D. J., Gillooly, K. M., Behnia, K., Schieven, G. L., Wityak, J., and Barrish, J. C. (2006). 2-Aminothiazole as a Novel Kinase Inhibitor Template. Structure-Activity Relationship Studies toward the Discovery of N-(2-Chloro-6-methylphenyl)-2-[[6-[4-(2-hydroxyethyl)-1-piperazinyl)]-2-methyl-4-pyrimidinyl]amino)]-1,3-thiazole-5-carboxamide (Dasatinib, BMS-354825) as a Potent pan-Src Kinase Inhibitor. J Med Chem *49*, 6819-6832.

Daub, H., Olsen, J.V., Bairlein, M., Gnad, F., Oppermann, F.S., Körner, R., Greff, Z., Kéri, G., Stemmann, O., and Mann, M. (2008). Kinase-Selective Enrichment Enables Quantitative Phosphoproteomics of the Kinome across the Cell Cycle. Molecular Cell *31*, 438-448.

Gallagher, T.F., Seibel, G. L., Kassis, S., Laydon, J. T., Blumenthal, M. J., Lee, J. C., Lee, D., Boehm, J. C., Fier-Thompson, S. M., Abt, J. W., Soreson, M. E., Smietana, J. M., Hall, R. F., Garigipati, R. V., Bender, P. E., Erhard, K. F., Krog, A. J., Hofmann, G. A., Sheldrake, P. L., McDonnell, P. C., Sanjay Kumar, S., Young, P. R., and Adams, J. L. (1997). Regulation of Stress-Induced Cytokine Production by Pyridinylimidazoles; Inhibition of CSBP Kinase. Bioorganic & Medicinal Chemistry *5*, 49-64.

Klutchko, S.R., Hamby, J. M., Boschelli, D. H., Wu, Z., Kraker, A. J., Amar, A. M., Hartl, B., G., Shen, C., Klohs, W. D., and Steinkampf, R. W., Driscoll, D. L., Nelson, J. M., Elliott, W. L., Roberts, B. J., Stoner, C. L., Vincent, P. W., Dykes, D. J., Panek, R. L., Lu, G. H., Major, T. C., Dahring, T. K., Hallak, H., Bradford, L. A., H. D. Hollis Showalter H. D. H., and Doherty, A. M. (1998). 2-Substituted Aminopyrido[2,3-d]pyrimidin-7(8H)-ones. Structure-Activity Relationships Against Selected Tyrosine Kinases and in Vitro and in Vivo Anticancer Activity. Journal of Medicinal Chemistry *41*, 3276-3292.

Langmead, B., Trapnell, C., Pop, M., & Salzberg, S. (2009). Ultrafast and memory-efficient alignment of short DNA sequences to the human genome. Genome Biology *10*, R25.

Mortazavi, A., Williams, B. A., McCue, K., Schaeffer, L., & Wold, B. (2008). Mapping and quantifying mammalian transcriptomes by RNA-seq. Nature Methods *5*, 621-628.

Ong SE, B.B., Kratchmarova I, Kristensen DB, Steen H, Pandey A, Mann M. (2002). Stable isotope labeling by amino acids in cell culture, SILAC, as a simple and accurate approach to expression proteomics. Mol Cell Proteomics *1*, 376-386.

Thingholm, T.E., Jørgensen, T.J., Jensen, O.N., Larsen, M.R (2006). Highly selective enrichment of phosphorylated peptides using titanium dioxide. Nature Protocols *1*, 1929-1935.

Supplemental Figure 1

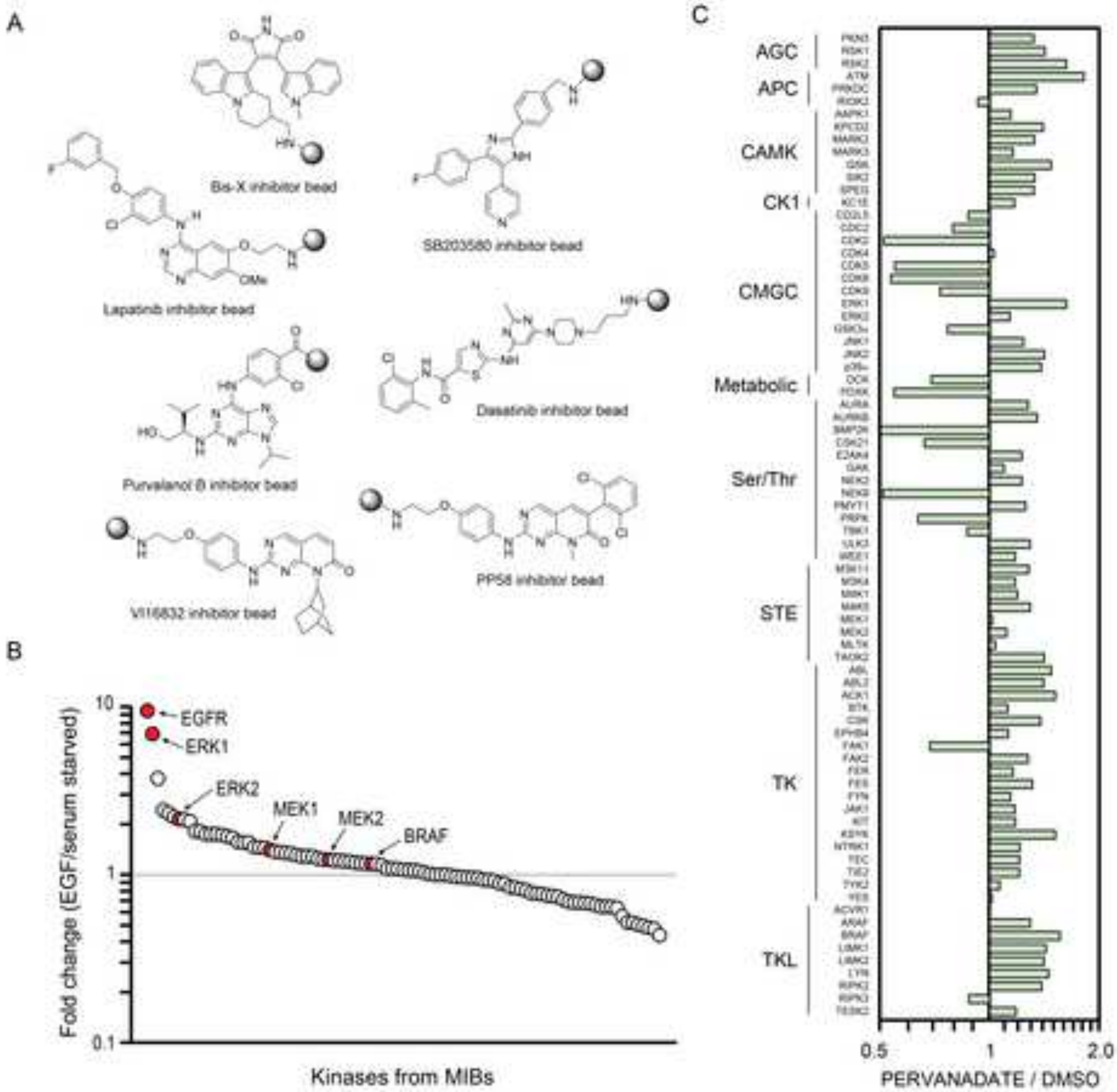

Duncan Figure S1

Supplemental Figure 2

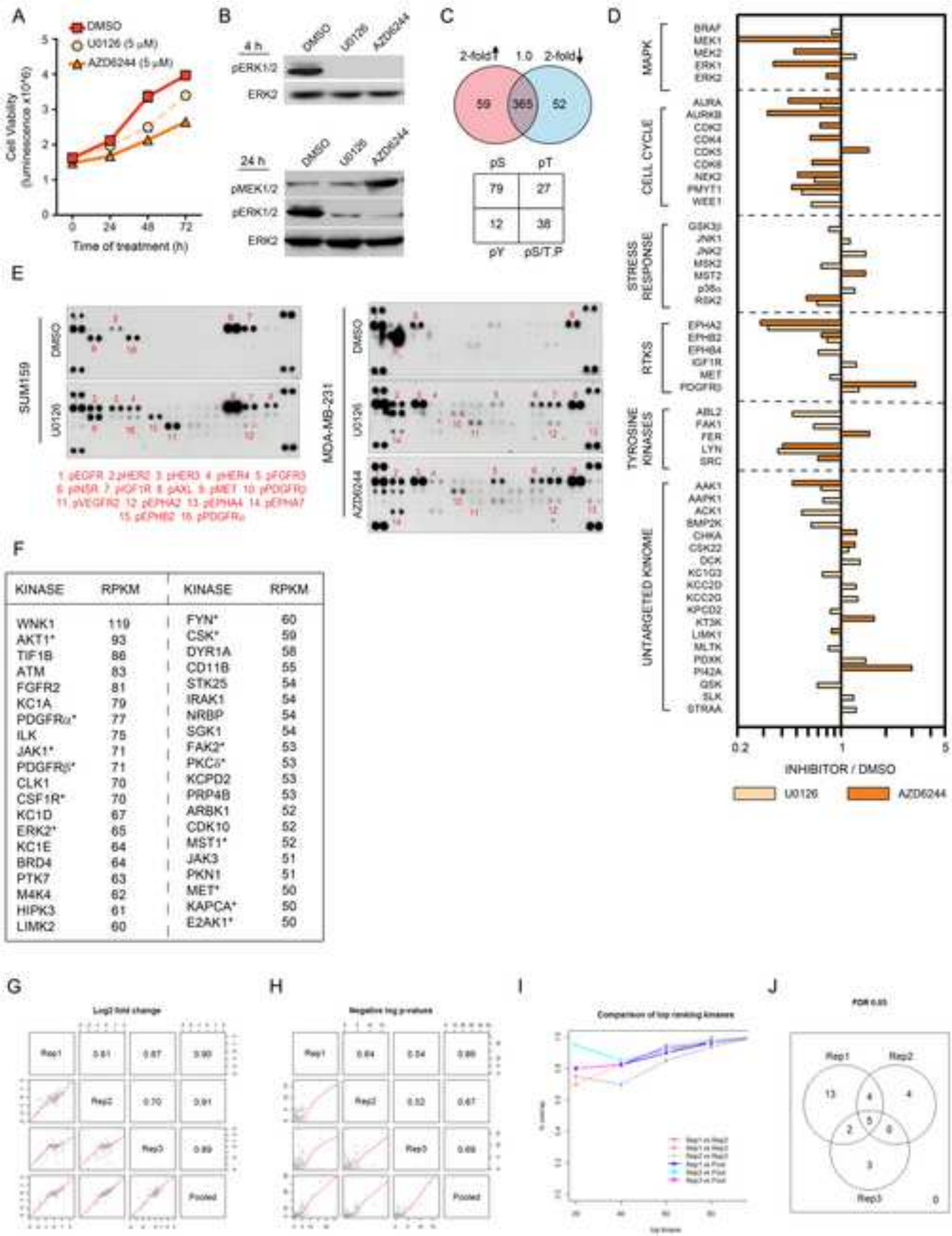

KINASE	RPKM	KINASE	RPKM
WNK1	119	FYN*	60
AKT1*	93	CSK*	59
TIF1B	86	DYR1A	58
ATM	83	CD11B	55
FGFR2	81	STK25	54
KC1A	79	IRAK1	54
PDGFRα*	77	NRBP	54
ILK	75	SGK1	54
JAK1*	71	FAK2*	53
PDGFRβ*	71	PKCδ*	53
CLK1	70	KCPD2	53
CSF1R*	70	PRP4B	53
KC1D	67	ARBK1	52
ERK2*	65	CDK10	52
KC1E	64	MST1*	52
BRD4	64	JAK3	51
PTK7	63	PKN1	51
M4K4	62	MET*	50
HIPK3	61	KAPCA*	50
LIMK2	60	E2AK1*	50

Duncan Figure S2

Supplemental Figure 3

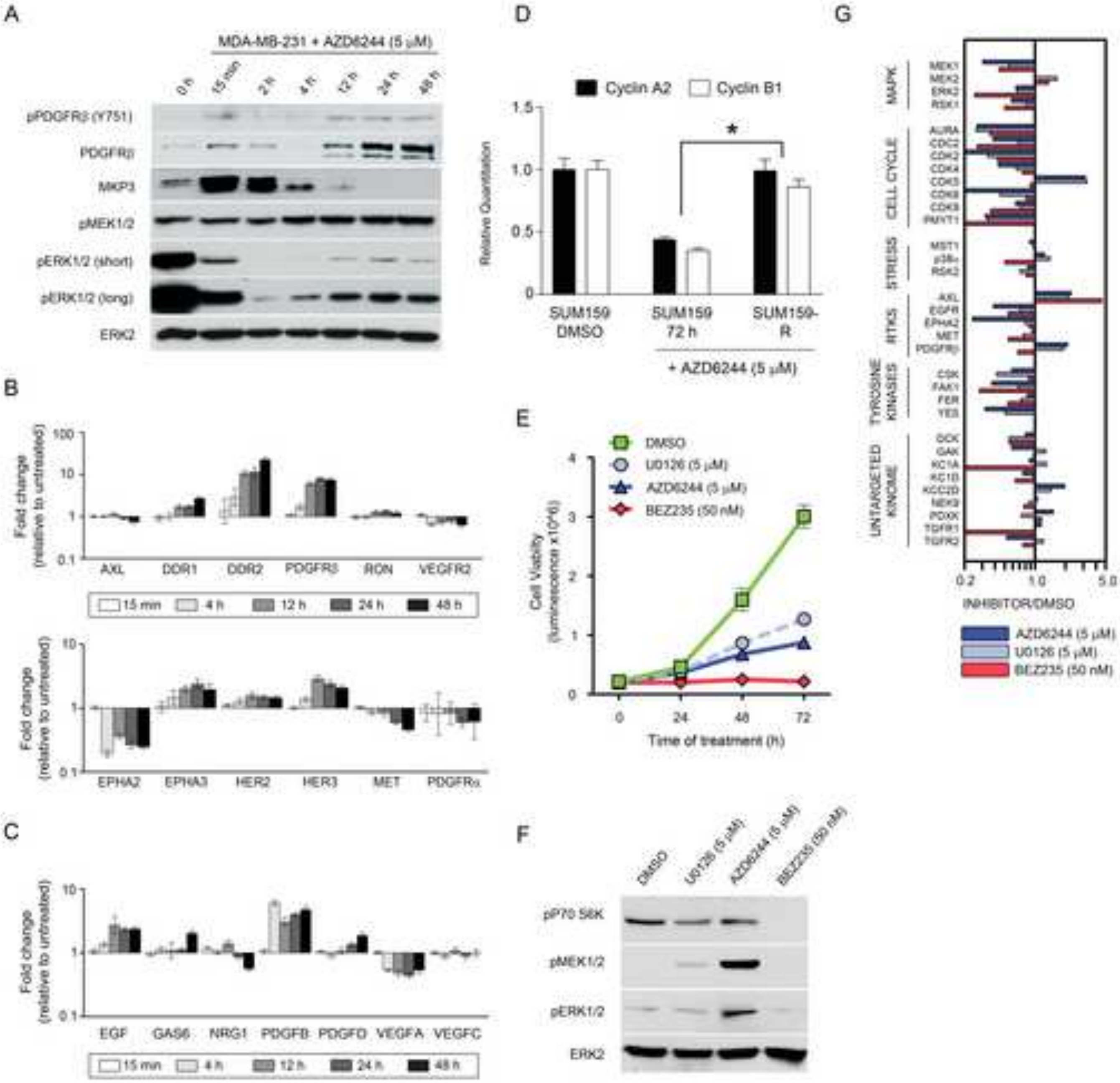

Duncan Figure S3

Supplemental Figure 4

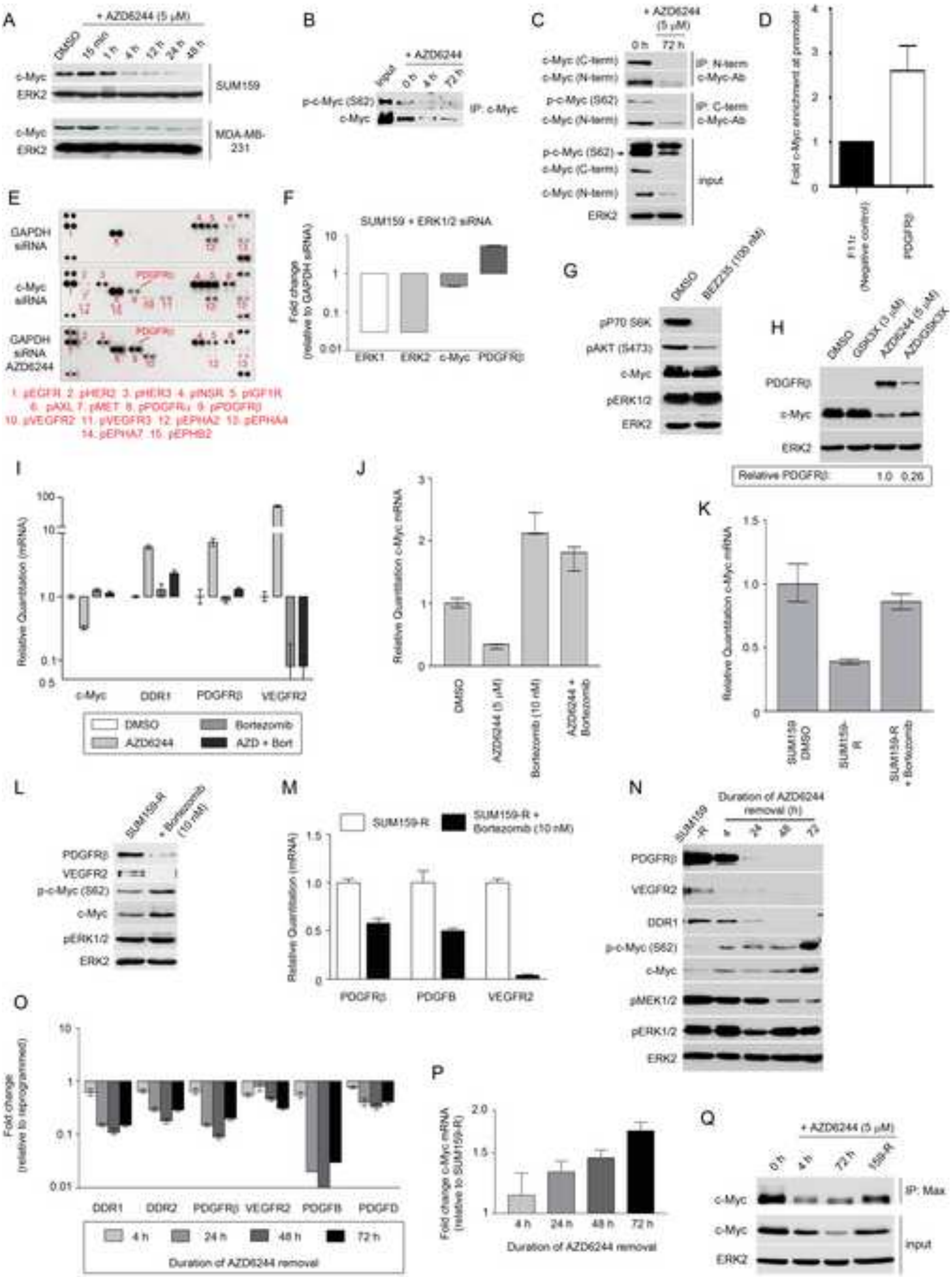

Duncan Figure S4

Supplemental Figure 5

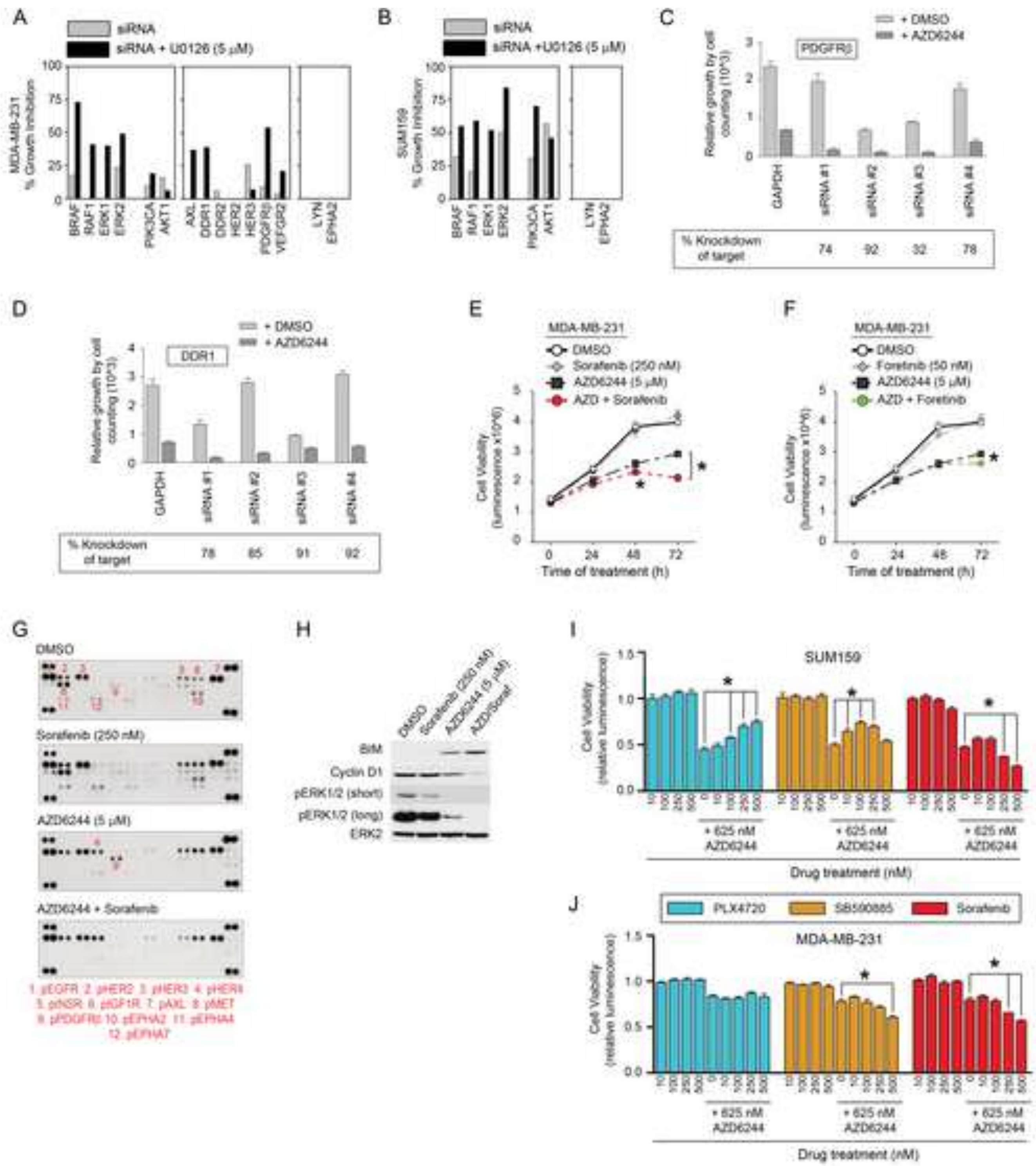

Duncan Figure S5

Supplemental Figure 6

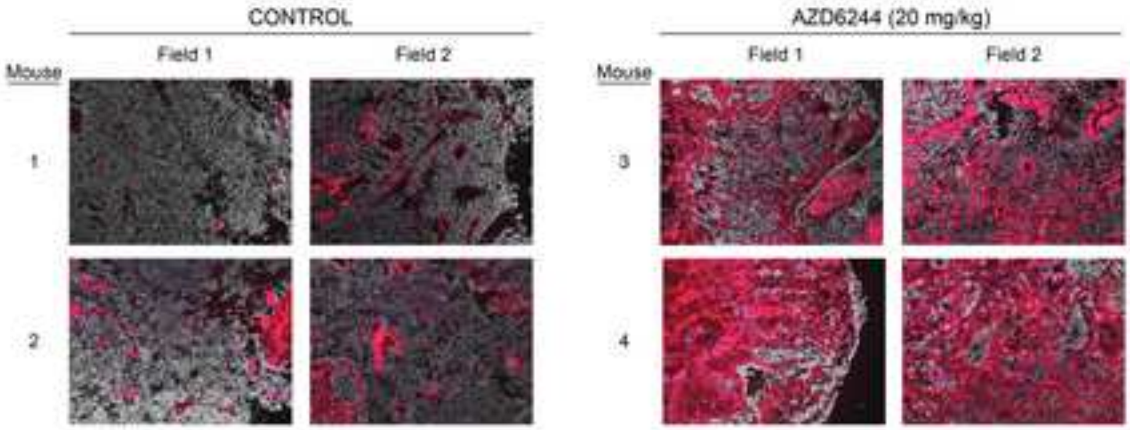

Duncan Figure S6

Supplemental Figure 7

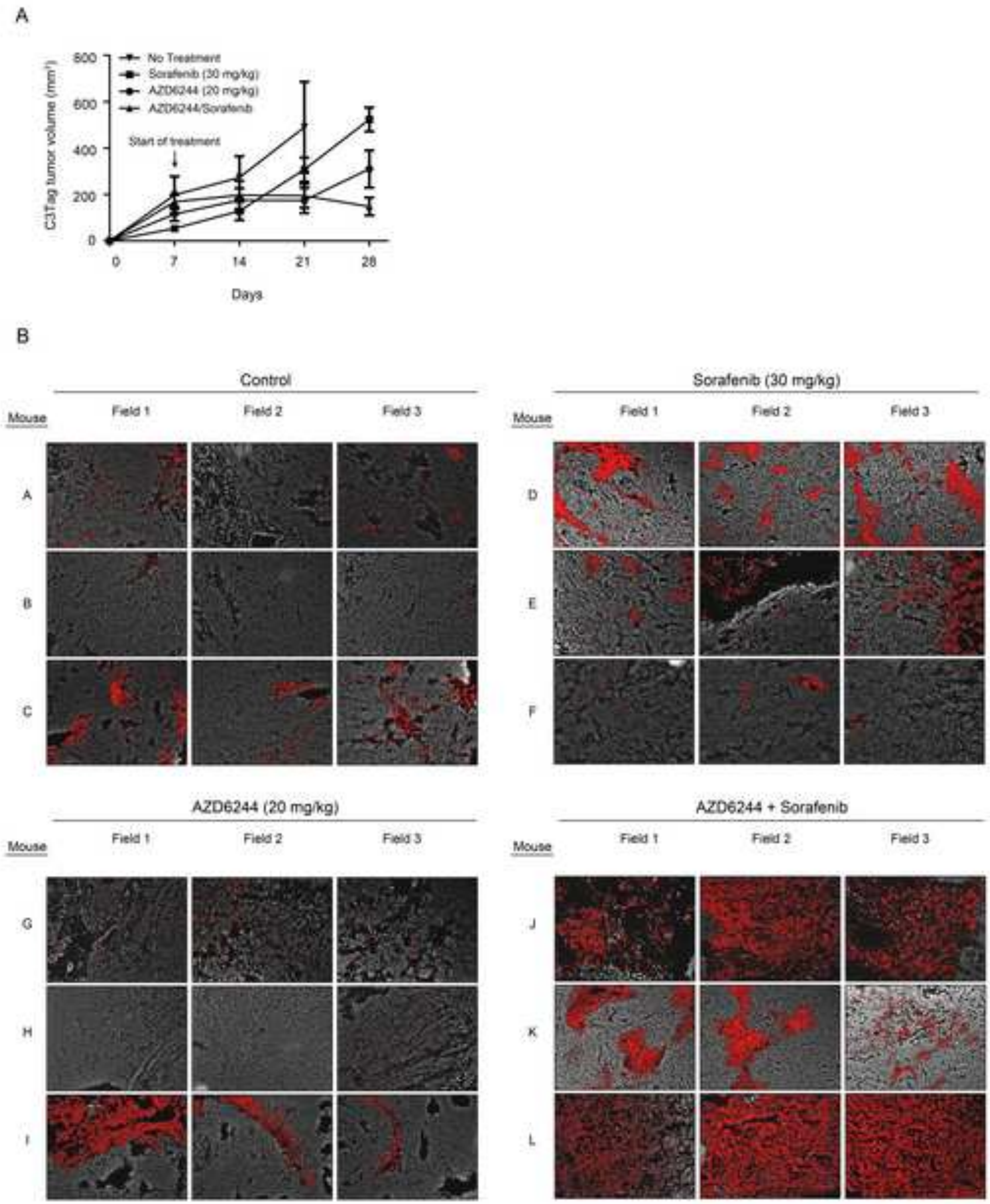

Duncan Figure S7